

The weak ferromagnetism of NiF₂

A. S. Borovik-Romanov, A. N. Bazhan, and N. M. Kreines

Institute of Physics Problems, USSR Academy of Sciences

(Submitted November 28, 1972)

Zh. Eksp. Teor. Fiz. 64, 1367-1382 (April 1973)

The magnetic properties of the antiferromagnetic crystal NiF₂ are investigated with a magnetometer with a vibrating sample at temperatures between 4.2 and 80°K for various magnetic field directions ($H_{\max} = 65$ kOe). The magnetization components perpendicular and parallel to the applied magnetic field are measured. For $T = 4.2^\circ\text{K}$ and $H \parallel [100]$ the usual linear dependence of the magnetic moment is observed (formula (4)). However, nonlinear growth of M is observed if H is inclined at an angle ψ ($0 < \psi < 45^\circ$) to the $[100]$ axis in the (001) plane. At $\psi = 45^\circ$ the $M(H)$ curve asymptotically approaches the straight line $M = \chi_{\perp} H$. This shows that on increase of H the antiferromagnetic vector L tends to become perpendicular to the field direction. The "transverse" weak ferromagnetism $\sigma_{D\perp}$ disappears in this case and a magnetic moment perpendicular to the magnetic field arises, the "longitudinal" weak ferromagnetism $\sigma_{D\parallel}$. The magnitudes of the "transverse" weak ferromagnetism $\sigma_{D\perp} = 169 \pm 2$ cgs cmu/mole and "longitudinal" weak ferromagnetism $\sigma_{D\parallel} = 57 \pm 4$ cgs cmu/mole are determined. The temperature dependences of $\sigma_{D\perp}$ and χ_{\perp} are studied. The data near T_N indicate that when $\chi_{\parallel} \approx \chi_{\perp}$ a consequence of the existence of "longitudinal" weak ferromagnetism is that the antiferromagnetic vector in a field applied along the $[110]$ axis becomes parallel to the magnetic field.

1. INTRODUCTION

The theory of weak ferromagnetism in antiferromagnets, developed by Dzyaloshinskii^[1,2], considers two models of the appearance of weak ferromagnetism. In the first model, the weak ferromagnetism is the result of the tilting of the magnetization vectors of the sublattices of the antiferromagnets ("transverse" weak ferromagnetism - $\sigma_{D\perp}$) and in the second the weak ferromagnetism is a consequence of the inequality of the sublattice magnetizations when they are exactly antiparallel ("longitudinal" weak ferromagnetism - $\sigma_{D\parallel}$). In all of the hitherto investigated weak ferromagnets (rhombohedral structures, orthoferrites, etc.), transverse weak ferromagnetism is observed. Among the known antiferromagnets, longitudinal weak ferromagnetism is possible in NiF₂. This is a tetragonal crystal (space group D_{4h}^{14} , which goes over below $T_N = 73.2^\circ\text{K}$ into an antiferromagnetic state with weak ferromagnetism^[3].

According to Dzyaloshinskii^[2], expansion of the thermodynamic potential in terms of the components of the magnetization vector M and the unit antiferromagnetism vector $\Delta = L/|L|$ for a crystal with NiF₂ symmetry is given by

$$\Phi = \frac{1}{2}a\Delta_x^2 + \frac{1}{2}bM_z^2 + \frac{1}{2}cM_x^2 - e(\Delta_x M_y + \Delta_y M_x) + \frac{1}{2}d(\Delta M)^2 - 2d(\Delta M)\Delta_x \Delta_y + \frac{1}{2}g\Delta_x^2 \Delta_y^2 - MH. \quad (1)$$

Neutron-diffraction data^[4] show that the vector L in NiF₂ is perpendicular to the fourfold axis. In this case, as shown by Dzyaloshinskii, two magnetic structures can exist in the absence of a magnetic field. In the first (Fig. 1a), the antiferromagnetic vector L is directed along one of the binary axes $[100]$ or $[010]$, and the magnetization vector M is directed respectively along the axis $[010]$ or $[100]$, i.e., it is perpendicular to L , and

$$M = \sigma_{D\perp} = \chi_{\perp} H_{D\perp} = e/B. \quad (2)$$

In the second structure (Fig. 1b), the vectors L and M are parallel to each other and are directed along one of the bisector axes $[110]$ or $[\bar{1}10]$. Here

$$M = \sigma_{D\parallel} = \chi_{\parallel} H_{D\parallel} = (e+d)/(B+D). \quad (3)$$

The static and resonant properties of NiF₂ were investigated experimentally and theoretically^[2-9]. The results of these investigations indicate that if the magnetic field is applied along the $[010]$ axis, then the first magnetic structure is realized starting already with relatively weak fields; this structure seems to be in equilibrium also in the absence of a magnetic field. Then

$$M = \sigma_{D\perp} + \chi_{\perp} H, \quad \chi_{\perp} = 1/B. \quad (4)$$

It is obvious that if a sufficiently strong external magnetic field is applied in the $[110]$ direction, then the antiferromagnetic vector L will tend to become perpendicular to the field and turn through an angle $\varphi = -\pi/4$ (or $\varphi = 3\pi/4$) from the $[100]$ axis (see Fig. 1c). Minimization of the potential (1) leads to the following equation, which connects the angle φ with the magnetic field applied along $[110]$:

$$\begin{aligned} (\cos \varphi - \sin \varphi) \{ 4[\chi_{\perp} H_{AE}^2 + \frac{1}{2}\chi_{\perp} H_{D\perp}^2 - \frac{1}{2}\chi_{\parallel} H_{D\parallel}^2] \sin 2\varphi (\cos \varphi + \sin \varphi) \\ + 2^{-1/2} [\sigma_{D\perp} - 2\sigma_{D\parallel} + 3(\sigma_{D\perp} - \sigma_{D\parallel}) \sin 2\varphi] H \\ + \frac{1}{2}\chi_{\perp} (1 - \chi_{\parallel} / \chi_{\perp}) H^2 (\cos \varphi + \sin \varphi) \} = 0; \end{aligned} \quad (5)$$

$$H_{AE}^2 = Bg, \quad \chi_{\parallel} = 1/(B+D), \quad H_{D\parallel} = e+d.$$

The magnetization of the crystal along the field is then expressed by

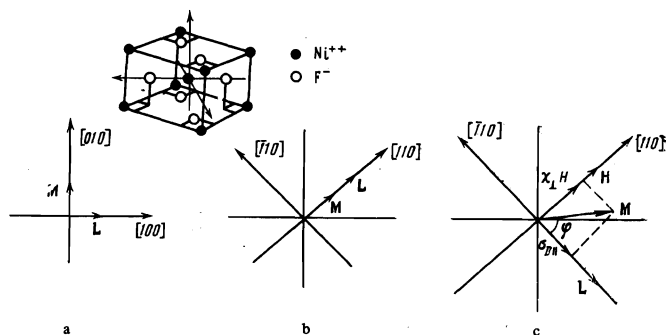


FIG. 1. Crystal lattice and possible magnetic states of NiF₂.

$$M_{\parallel} = 2^{-1/2} [\sigma_{D\perp} - (\sigma_{D\perp} - \sigma_{D\parallel}) \sin 2\varphi] (\cos \varphi + \sin \varphi) + 1/2 \chi_{\perp} H [(1 + \chi_{\parallel} / \chi_{\perp}) - (1 - \chi_{\parallel} / \chi_{\perp}) \sin 2\varphi]. \quad (6)$$

As $\varphi \rightarrow \pi/4$ (or $\varphi \rightarrow 3\pi/4$) we get $M_{\parallel} = \chi_{\perp} H$.

From the minimum of (1) we can also determine the crystal-magnetization component in a direction perpendicular to the field applied along [110]:

$$M_{\perp} = 2^{-1/2} [\sigma_{D\perp} + (\sigma_{D\perp} - \sigma_{D\parallel}) \sin 2\varphi] (\cos \varphi - \sin \varphi) + 1/2 \chi_{\perp} H (1 - \chi_{\parallel} / \chi_{\perp}) \cos 2\varphi. \quad (7)$$

Thus, if a "longitudinal" weak ferromagnetism $\sigma_{D\parallel}$ exists in the substance, it should contribute to the magnetization in the direction perpendicular to the applied field. As $\varphi \rightarrow \pi/4$ (or $\varphi \rightarrow 3\pi/4$), as seen from (7), we have $M_{\perp} = \sigma_{D\parallel}$.

At the given constants that enter in the thermodynamic potential, and at the given value of the magnetic field $H \parallel [110]$, that state of the crystal which corresponds to the minimum of the thermodynamic potential (1) is realized. In terms of the new notation, formula (1) becomes

$$\Phi = -1/2 \chi_{\perp} H D_{\perp}^2 + [\chi_{\perp} H A E^2 + 1/2 \chi_{\perp} H D_{\perp}^2 - 1/2 \chi_{\parallel} H D_{\parallel}^2] \sin^2 2\varphi - 2^{-1/2} \sigma_{D\perp} H (\cos \varphi + \sin \varphi) + 2^{-1/2} [\sigma_{D\perp} - \sigma_{D\parallel}] H (\cos \varphi + \sin \varphi) \sin 2\varphi - 1/2 \chi_{\perp} H^2 (1 + \chi_{\parallel} / \chi_{\perp}) + 1/2 \chi_{\perp} H^2 (1 - \chi_{\parallel} / \chi_{\perp}) \sin 2\varphi. \quad (1a)$$

The purpose of the present study was to investigate the rotation of the vectors of the antiferromagnetic sublattices in NiF_2 under the influence of the field and to observe the "longitudinal" weak ferromagnetism.

2. APPARATUS AND SAMPLES

The magnetic properties of single-crystal NiF_2 were investigated with a modified Foner magnetometer^[10] with a vibrating sample in magnetic fields up to 65 kOe and in the temperature interval from 4.2 to 80°K. To measure the magnetization of the sample, both in the direction of the magnetic field and perpendicular to it, we used two pairs of measuring coils, L1 and L2, the axes of which were parallel to the direction of motion of the sample (see Fig. 2). Sample 1 vibrated on holder 2, which was coupled to an electrodynamic vibrating system. The vibration frequency was $\nu = 73$ Hz, and the vibration amplitude was ~ 1 mm. The sample, together with the holder and the vibrating system, could be rotated about the vertical axis relative to the system of the superconducting coils producing the magnetic field and relative to the measuring coils. To produce temperatures intermediate between 4.2 and 80°K, a rod 3 of single-crystal quartz having good thermal conductivity was glued between the sample and the holder. A heater was wound around the rod, and a thermocouple of iron-doped gold and chromel was glued to the rod. The sample was placed in vacuum jacket 4 together with the holder and the vibrating system.

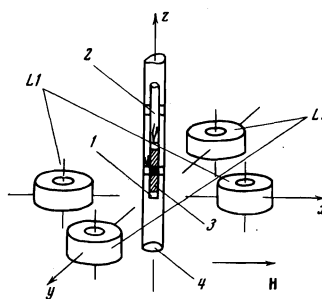


FIG. 2. Schematic diagram of the arrangement of the measuring coils L1 and L2 in the instrument: 1—sample, 2—holder, 3—quartz rod, 4—vacuum jacket.

The signal from the measuring coil L1, or L2, which was proportional respectively to the projection of the magnetization of the sample on the direction parallel to the magnetic field (M_{\parallel}) and perpendicular to it (M_{\perp}), was fed to a tuned amplifier and then through a synchronous detector to the Y coordinate of a two-coordinate potentiometer. The signal applied to the X coordinate of this potentiometer was proportional to the current through the superconducting solenoid.

In fields exceeding 6 kOe, the dependence of the magnetic field on the current in the superconducting coils was linear with accuracy better than 1%. The solenoid was calibrated with the aid of a Hall pickup adapted to operate at helium temperatures^[1]. In fields weaker than 6 kOe it is necessary to take into account the hysteresis of the superconducting coils due to the "frozen-in" annular currents. To this end, calibration curves of the magnetization of single-crystal MnF_2 ($H \perp [001]$) were plotted as functions of the current in the superconducting coils ($M_{\parallel} = \chi_{\perp} H$). The residual field at zero current in our solenoid was 200 Oe. The magnetometer was also calibrated with the aid of an MnF_2 single crystal by measuring its magnetization in strong fields.

NiF_2 samples in the form of nearly-cubic parallelepipeds with dimension ~ 1 mm were cut from single crystals grown by S. V. Petrov. The samples were oriented with an x-ray goniometer. The accuracy of sample orientation was $\sim 2-3^\circ$.

3. MEASUREMENT RESULTS

A. Temperature $T = 4.2$ K

Figure 3 shows the dependence of the magnetic moment of NiF_2 on the field at $H \parallel [001]$ and $H \parallel [010]$. In the former case this dependence is given by

$$M = \chi_{\perp} H, \quad \chi_{\perp} = (5.9 \pm 0.1) \cdot 10^{-3} \text{ cgs emu/mole}$$

In the latter case, in fields exceeding 4–5 kOe, we have

$$M = \sigma_{D\perp} + \chi_{\perp} H, \quad \sigma_{D\perp} = 169 \pm 2 \text{ cgs emu/mole} \\ \chi_{\perp} = (6.2 \pm 0.1) \cdot 10^{-3} \text{ cgs emu/mole}$$

In all the succeeding measurements, the sample was mounted in such a way that the [001] axis was parallel to the suspension, and the magnetic field was always in the basal plane and could be directed at an arbitrary angle ψ relative to the [010] axis.

To study the mechanism of magnetization reversal in relatively weak fields, we investigated the field dependences of the magnetic moments M_{\parallel} and M_{\perp} parallel and perpendicular to the field, respectively, for differ-

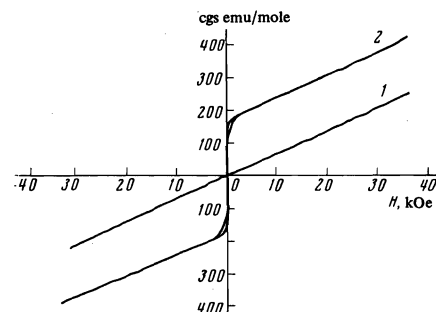


FIG. 3. Plots of $M(H)$ at $H \parallel [001]$ (line 1) and $H \parallel [010]$ (curve 2); $T = 4.2^\circ\text{K}$.

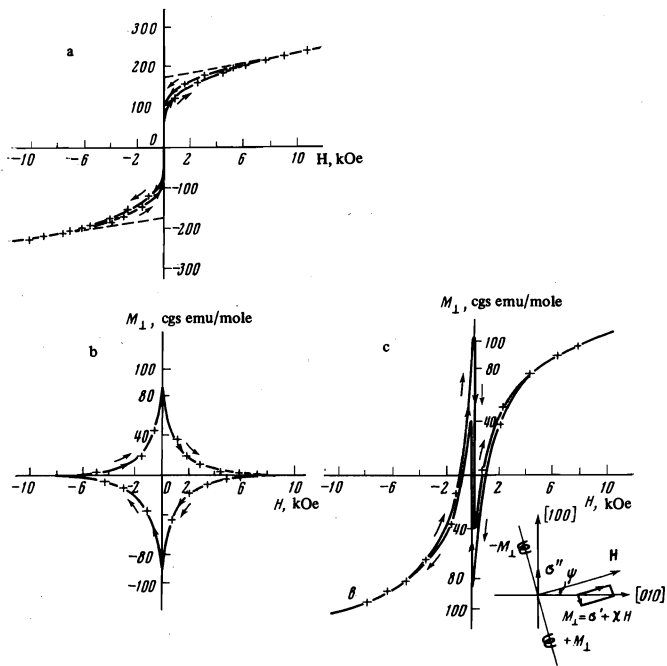


FIG. 4. Plots of $M_{\parallel}(H)$ and $M_{\perp}(H)$ in the course of reversal of the crystal magnetization (the arrows indicate the direction of the magnetization reversal): a, b— $\psi = 0$, c— $\psi = 20^{\circ}$.

ent field directions. Figure 4a shows a plot of $M_{\parallel}(H)$ for $\psi = 0^{\circ}$. We see that within the accuracy of our measurements (~ 20 – 40 Oe), approximately half of the ferromagnetic moment is reversed jumpwise when the sign of the field is reversed. Complete saturation sets in at field strength 5–6 kOe. Figure 4b shows the behavior of M_{\perp} .

It should be noted that the sign of the moment M_{\perp} in these measurements depended on the sign of ψ relative to the $[010]$ axis. A change of a fraction of a degree in ψ , in either direction relative to $\psi = 0$, always yielded a hysteresis cycle of the same time that differed only in the sign of M_{\perp} , or, equivalently, in the circuiting direction of the cycle. We did not succeed in establishing intermediate angles ψ at which a smooth transition could be observed from one picture to another. When the field decreased from a value exceeding 10 kOe, the direction of M_{\perp} always coincided with the direction of the projection of the magnetic field on the $[100]$ axis. This was confirmed in experiment with an angle $-\psi = 20^{\circ}$. In this case (see Fig. 4c), in not too strong a field $H > 0$, the magnetization is directed along the $[010]$ axis and its projection on the direction of the perpendicular coils is directed downward (Fig. 4c). This direction was taken by us to be the positive direction of M_{\perp} . When the field decreased to zero, as seen from Fig. 4c, M_{\perp} becomes negative, i.e., as stated above, it is directed to the same side as the projection of the field on the $[100]$ axis. We note that at $\psi \approx 0$ the value of M_{\perp} is also close to half the total magnetic moment of the sample.

We proceed now to describe the results obtained in strong magnetic fields. Figure 5a shows plots of $M_{\parallel}(H)$ for different angles ψ between the direction of the magnetic field and the $[010]$ axis. It is seen from the figure that when the angle ψ is varied the character of the magnetization curves in strong fields is altered. With increasing angle ψ , the relation $M_{\parallel} = \sigma' + \chi'H$ ceases

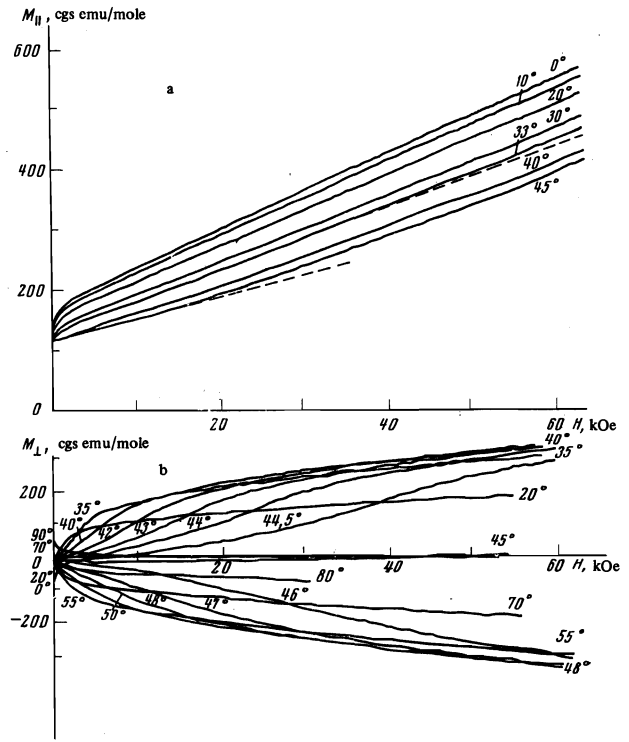


FIG. 5. Plots of $M_{\parallel}(H)$ and $M_{\perp}(H)$ against the angle ψ between the magnetic field H and the $[010]$ axis.

to hold, and the magnetization begins to increase in nonlinear fashion. There is also a significant change in the initial section of the magnetization curve, namely, the region of sharp increase of the magnetization in weak fields disappears.

It should be indicated that the value of the magnetic moment σ' measured at different angles ψ becomes equal, as $H \rightarrow 0$, to the projection of the spontaneous magnetic moment, fixed on the $[010]$ axis, on the direction of the field and of the measuring coils. At $-\psi = 45^{\circ}$ we have $\sigma' = 2^{-1/2} \sigma_{D_{\perp}}$, where $\sigma_{D_{\perp}}$ is the total magnetic moment at $\psi = 0$. Figure 5b shows plots of $M_{\perp}(H)$ for different angles ψ . At $\psi = 0$ in strong fields we have $M_{\perp} = 0$. With increasing angle ψ , the values of M_{\perp} increase. The spontaneous magnetic moment σ' then increases like the projection of the total spontaneous magnetic moment on the axis perpendicular to H . Starting with angles $-\psi = 40^{\circ}$, the values of M_{\perp} in the strong field practically coincide, but the initial sections of the magnetization curves are strongly stretched out along the field, so that at $-\psi = 44^{\circ}$ the merging with the curve for $-\psi = 40^{\circ}$ is reached in a field ~ 65 kOe. At $-\psi = 45^{\circ}$, M_{\perp} is close to zero in the entire range of strong fields. At $\psi > 45^{\circ}$, the sign of M_{\perp} is reversed, and on the whole all the curves for the corresponding angles $90^{\circ} - \psi$ are symmetrical images of the curves for the angles ψ , with the sign reversed.

B. The Temperature Range 4.2–80 K

In the wide range of temperatures from 4.2 to 80°K , we investigated the functions $M_{\parallel}(H)$ and $M_{\perp}(H)$ for different angles ψ . Figure 6 shows plots of $M_{\parallel}(H)$ for a number of temperatures. The character of the $M_{\parallel}(H)$ dependence for $\psi = 0$ ($H \parallel [010]$) remains the same at all temperatures, and by reducing curves of this type, plotted at different temperatures, we obtained the tem-

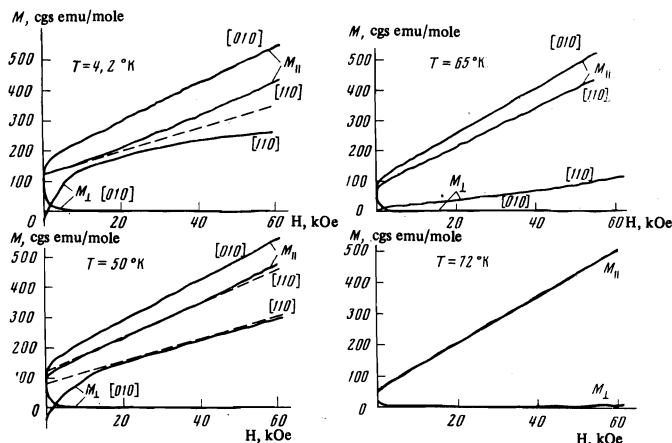


FIG. 6. Plots of $M_{\parallel}(H)$ and $M_{\perp}(H)$ against the temperature for two directions of the field, $H \parallel [010]$ and $H \parallel [110]$ (the corresponding axes are marked on the curves).

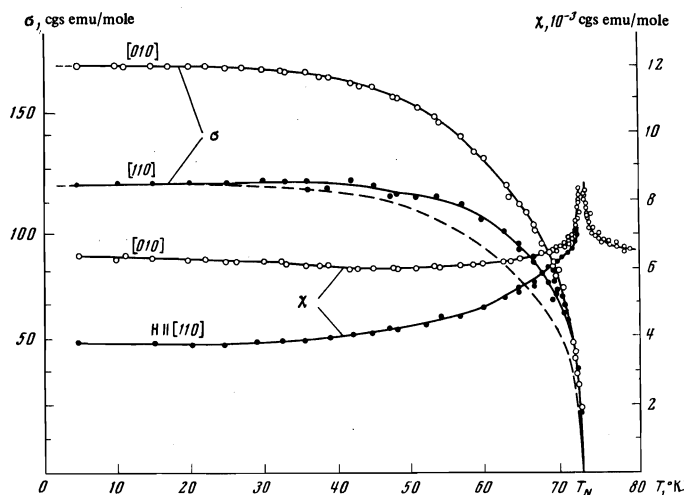


FIG. 7. Temperature dependences of $\sigma_{\perp}(T)$ and $\chi_{\perp}(T)$ at $H \parallel [010]$ and $\sigma'(T)$ and $\chi'(T)$ at $H \parallel [110]$. The dashed curve shows the dependence of $\sigma_{\perp}(T)\sqrt{2}/2$, corresponding to a model wherein the spontaneous magnetic moment $\sigma_{\perp}(T)$ is fixed on the $[010]$ axis.

perature dependences $\sigma_{\perp}(T)$ and $\chi_{\perp}(T)$ shown in Fig. 7. The magnetic susceptibility changes little in the entire range of temperatures, with the exception of the vicinity of the temperature $T_N = 73.3^\circ\text{K}$, at which a sharp maximum of the susceptibility is observed. The spontaneous moment σ_{\perp} vanishes at the same temperature.

The $M_{\parallel}(H)$ curves for $\psi = 45^\circ$ ($H \parallel [110]$) experience a significant change in form in the temperature region near 50°K . In weak fields, there appear on the curves sections in which the magnetization increases rapidly, similar to the effect observed on the $M_{\parallel}(H)$ curves at $\psi = 0$. This is followed by a rather large section where the magnetization increases linearly with the field. The region of nonlinear growth of the magnetization with increasing temperature shifts towards stronger magnetic fields. The values of the spontaneous magnetic moment σ' , measured at angles ψ different from zero (the method of determining σ' is given below) become larger than the corresponding value of the projection of the spontaneous magnetic moment fixed along the $[010]$ axis (see Fig. 7). Starting with a temperature $\sim 72^\circ\text{K}$ the magnetization curves plotted at different angles ψ practically coincide.

Figure 7 also shows the values of $\sigma'(T)$ and $\chi'(T)$ obtained by reducing the linear sections of the $M_{\parallel}(T)$ curves for $\psi = 45^\circ$ at temperatures higher than 50°K . The values of σ' for temperatures below 50°K , shown in this plot, are directly the values of $M_{\parallel}(H)$ for $\psi = 45^\circ$ at $H = 0$. No anisotropy of the magnetic susceptibility was observed in the (001) plane at temperatures above T_N .

Figure 6 also shows plots of $M_{\perp}(H)$ at $\psi = 40^\circ$ (" $H \parallel [110]$ ") at different temperatures. It is seen from the figure that at temperatures above 50°K the character of these curves also changes. In weak fields, an appreciable decrease takes place in the spontaneous magnetic moment σ'_{\perp} . Its magnitude becomes smaller than the projection of the magnetic moment on this direction (if the magnetic moment is fixed on the $[010]$ axis), corresponding to the given temperature, and the contribution to M_{\perp} is determined in the main by the magnetic susceptibility. At $T > 71^\circ\text{K}$, the $M_{\perp}(H)$ signal drops to zero. At $T \approx 72^\circ\text{K}$, the moment $M_{\perp}(H)$ is close to zero at all angles ψ and at all values of the magnetic field H .

4. DISCUSSION OF RESULTS

1. In agreement with the earlier studies, we have found that if the magnetic field is applied along the axes $[010]$ and $[001]$, then NiF_2 exhibits the characteristic properties of an antiferromagnet with weak ferromagnetism. The values obtained by us for χ_{\perp}^* , χ_{\perp} , and σ_{\perp} , coincide within the limits of error with the values obtained in^[3,7] (see the table below). From these values we can obtain the effective exchange field $H_E = 1170 \pm 20$ kOe and the Dzyaloshinskiĭ field $H_{D_{\perp}} = 27.2 \pm 0.2$ kOe.

2. From an examination of the results shown in Figs. 4 and 5 we can draw the following conclusions concerning the picture of magnetization reversal in NiF_2 . In the absence of a magnetic field, the sample is broken up into domains of four types, with spontaneous magnetizations directed along the perpendicular binary axes $[100]$, $[010]$ and $[\bar{1}00]$, $[0\bar{1}0]$.

If the magnetic field H is applied along the $[010]$ axis (in practice the accuracy of orientation of H relative to the crystallographic axes is $\sim 1^\circ$), then the crystal goes over in relatively weak fields (~ 20 Oe) into a two-domain state, with mutually perpendicular spontaneous magnetizations directed along the axes $[100]$ and $[010]$ or $[\bar{1}00]$ and $[010]$ (the direction of the magnetization perpendicular to the magnetic field, $[100]$ or $[\bar{1}00]$, depends on the sign of the angle between H and the $[010]$ axis). The summary volumes of the domain regions of each sort are equal in magnitude. With further increase of the magnetic field, the crystal goes over into a single-domain state with spontaneous magnetization along the magnetic field in fields ~ 7 kOe.

On the other hand, if the magnetic field is applied along the $[110]$ axis, then the crystal, going over in weak fields (~ 100 Oe) into a two-domain state with equal magnetizations directed along the axes $[100]$ and $[010]$, remains in this state at all values of the magnetic field, inasmuch as in this case the two domains have equal energies in the magnetic field. If the magnetic field is directed at a certain angle ψ (for example, $\psi = 20^\circ$ - Fig. 4c), then magnetization gives rise to a change in the sign of M_{\perp} , thus confirming the fact that

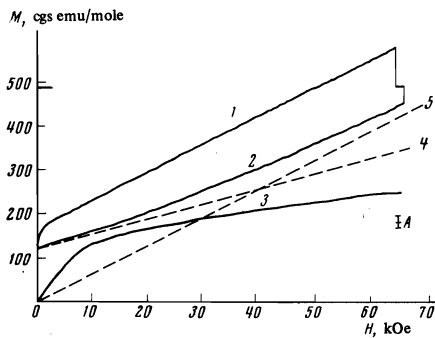


FIG. 8. Plot of $M_{\parallel}(H)$ at $H \parallel [010]$ (curve 1) and at $H \parallel [110]$ (curve 2) and dependence of $M_{\perp}(H)$ at $H \parallel [110]$ (angle $\psi = 40^\circ$) (curve 3). The dashed lines are plots of $M_{\parallel}(H)$ in the following limiting states: curve 4—according to (8), when the antiferromagnetic vector L is fixed on the $[100]$ axis, curve 5— $M_{\perp} = \chi_{\perp} H$, when $L \perp H$.

in weak fields the crystal is broken up into two mutually perpendicular domains, the magnetization projections of which on the axis of the perpendicular coils are oppositely directed. At angles $-\psi$ close to 45° , i.e., when the direction of the magnetic field is close to the $[110]$ axis, the magnetization reversal to the one-domain state takes place in stronger fields, for example, at $-\psi = 40^\circ$ (Fig. 5b) the crystal is in a single-domain state only in fields exceeding ~ 10 kOe.

For the theoretical estimates, we shall henceforth discuss the results for M_{\parallel} at $-\psi = 45^\circ$ and for M_{\perp} at $-\psi = 40$ and 42° .

3. Figure 8 shows plots of $M_{\parallel}(H)$ at $H \parallel [010]$ and $H \parallel [110]$. The figure also shows a plot of

$$M_{\parallel} = 2^{-1/2} \sigma_{D_{\perp}} + 1/2 \chi_{\perp} H \quad (8)$$

which describes the course of the magnetization for the model wherein the spontaneous magnetic moment at $H \parallel [110]$ is fixed on the $[010]$ axis. It is seen from the figure that the straight line plotted in accordance with this formula does not agree with the experimental curve. With increasing magnetic field, the differential magnetic susceptibility χ' increases in comparison with $\chi_{\perp}/2$, and in a field of 65 kOe we have $\chi'/\chi_{\perp} = 0.9 \pm 0.04$; on the other hand, the projection of the quasi-spontaneous magnetic moment σ' , intercepted by the tangent to the $M_{\parallel}(H)$ curve on the ordinate axis, decreases with increasing magnetic field, and at $H = 65$ kOe we have the ratio $\sigma'/\sigma_{D_{\perp}} = 0.30 \pm 0.02$. Figure 8 also shows the line $M_{\parallel} = \chi_{\perp} H$ along which the magnetization should vary if $L \perp H$. We see that the experimental magnetization curve comes close to this line.

On the basis of these data and the data given in Sec. 3, we can conclude that at $H \parallel [010]$, and at arbitrary H directions in weak fields, the spontaneous magnetic moment is directed along the $[010]$ axis, while the antiferromagnetic vector L is directed along the $[100]$ axis. With increasing magnetic field at $H \parallel [110]$, the antiferromagnetic vector L tends to rotate perpendicular to the direction of the magnetic field, and then the spontaneous magnetic moment due to the transverse weak ferromagnetism vanishes. The same Fig. 8 shows the experimental plot of $M_{\perp}(H)$ at $\psi = 40^\circ$. It is seen from the figure that in strong magnetic fields the experimental curve deviates from the line (8). However, the deviation of the experimental curve is much smaller than the one expected as a result of the devia-

tion of L in the absence of a parallel weak ferromagnetism.

From a comparison of the experimental $M_{\parallel}(H)$ and $M_{\perp}(H)$ curves we can draw the qualitative conclusion that a "longitudinal" weak ferromagnetism exists in NiF_2 . Indeed, taking (6) and (7) into account and neglecting the value of χ'_{\parallel} (relative to χ_{\perp}), we can estimate from the ratio χ'/χ_{\perp} (Fig. 8) the angle φ between L and the $[100]$ axis ($\varphi \sim 22^\circ$) and the contribution of the paramagnetic moment $\chi_{\perp} H$ to $M_{\perp}(H)$ corresponding to this angle. Further if it is assumed that there is no longitudinal weak ferromagnetism, then the spontaneous magnetic moment is always perpendicular to the antiferromagnetic vector. From the ratio $\sigma'/\sigma_{D_{\perp}}$ we can then estimate the contribution made to $m_{\perp}(H)$ by the projection $\sigma'_{D_{\perp}}$. The point A in Fig. 8 marks the value of M_{\perp} at $H = 65$ kOe that could be expected on the basis of estimates made in this manner. We see that the assumption that there is no "longitudinal" weak ferromagnetism does not agree with the values obtained by us for M_{\parallel} and M_{\perp} in strong fields. We see also that the contribution of the "longitudinal" weak ferromagnetism amounts to $\sim 20\%$ of the observed total magnetic moment.

4. For a quantitative comparison of the obtained experimental curves with theory it is necessary to obtain the theoretical dependence of $M_{\parallel}(H)$ and $M_{\perp}(H)$ for the case when the magnetic field is directed along the $[110]$ axis. To this end it is necessary to solve Eq. (5), to find the $\varphi(H)$ dependence, and to substitute it in formulas (6) and (7). By varying the parameters HAE , χ_{\parallel} , and $H D_{\parallel}$ we must find their optimal values, those which give the best agreement with the experimental $M_{\parallel}(H)$ and $M_{\perp}(H)$ curves. However, the performance of such a program is exceedingly complicated and does not make it possible to determine the indicated parameters uniquely. We have therefore used additional data on antiferromagnetic resonance (AFMR) in NiF_2 , as obtained by Richards^[5].

In the case of NiF_2 , the AFMR frequencies cannot be calculated by the usual method in which the Landau-Lifshitz equation is used for the magnetic sublattices, since the condition $\Delta \cdot M = \text{const}$, which is needed to be able to write down the Landau-Lifshitz equations, is not satisfied in the case of oscillations of the vectors Δ and M . This is seen from the expression obtained by minimizing (1)

$$\Delta M = 2 \frac{e+d}{B+D} \Delta_x \Delta_y + \frac{H \Delta}{B+D}. \quad (9)$$

Turov^[9] has proposed a phenomenological model in which this difficulty is circumvented in the following manner. The Dzyaloshinskii thermodynamic potential is written not for the magnetic but for the spin mechanical moments l and m :

$$l = (I_1 - I_2) / I_0, \quad m = (I_1 + I_2) / I_0,$$

where I_i is the vector of the mechanical moments of the sublattices, and I_0 is its absolute magnitude. It was proposed that the vectors l and m satisfy the conditions $l \cdot m = 0$ and $l^2 + m^2 = 1$, and that their connection with the magnetic moments be described by $g_{\alpha, \beta}^{(i)}$ tensors that take into account the local symmetry of the magnetic Ni^{2+} ions in each of the two sublattices ($i = 1, 2$). For the components of the magnetization vector M , this connection takes the following form:

$$M_x = M_0 g_{\perp} (m_x + \tau l_x), \quad M_y = M_0 g_{\perp} (m_y + \tau l_y), \quad M_z = M_0 g_{\parallel} m_z. \quad (10)$$

Here $\tau = g_{xy}/g_{\perp}$ and $M_0 = \mu_B I_0$ (μ_B is the Bohr magneton).

Taking the foregoing into account, the thermodynamic potential takes the form

$$\Phi = \frac{1}{2} a' l_x^2 + \frac{1}{2} A m^2 + \frac{1}{2} b' m_z^2 - q (l_x m_y + l_y m_x) + \frac{1}{2} l_z^2 l_y^2 - \frac{H_x}{g_{xx} M_0} (m_x + \tau l_x) - \frac{H_y}{g_{yy} M_0} (m_y + \tau l_y) - \frac{H_z}{g_{zz} M_0} m_z. \quad (11)$$

Introducing in place of l_x and l_y the angle φ of the rotation of the vector l away from the [100] axis and minimizing the potential for the case $H \parallel [010]$, Turov obtained for the magnetization a formula that coincides with (4), where

$$\sigma_{D\perp} = M_0 g_{\perp} (q/A + \tau), \quad \chi_{\perp} = g_{\perp}^2 M_0^2 / A, \quad (12)$$

and an expression for the longitudinal weak ferromagnetism, which is connected with the anisotropy of the tensors $g_{\alpha\beta}^1$ of the magnetic ions of different sublattices:

$$M = \sigma_{D\parallel} = M_0 g_{\perp} \tau. \quad (13)$$

For the frequency of the lower AFMR branch in NiF_2 , Turov^[9] obtained the following expression:

$$(\omega/\gamma)^2 = 8[H_{AE}^2 + \frac{1}{2}(H_{D\perp} - H_{\tau})^2] + H^2 + H(5H_{D\perp} - 4H_{\tau}); \quad (14)$$

$$H_{\tau} = \tau A, \quad H_{D\perp} = q + \tau A, \quad H_{AE}^2 = Af.$$

We have minimized the potential (11) for the case $H \parallel [110]$ and obtained the following expression connecting the angle φ with the applied field:

$$(\cos \varphi - \sin \varphi) \{4[\chi_{\perp} H_{AE}^2 + \frac{1}{2} \chi_{\perp} (H_{D\perp} - H_{\tau})^2] \sin 2\varphi (\cos \varphi + \sin \varphi) + 2^{-1/2} [\sigma_{D\perp} - 2\sigma_{D\parallel} + 3(\sigma_{D\perp} - \sigma_{D\parallel}) \sin 2\varphi] H + \frac{1}{2} \chi_{\perp} H^2 (\cos \varphi + \sin \varphi)\} = 0 \quad (15)$$

and expressions for the magnetization components

$$M_{\parallel} = 2^{-1/2} [\sigma_{D\perp} - (\sigma_{D\perp} - \sigma_{D\parallel}) \sin 2\varphi] (\cos \varphi + \sin \varphi) + \frac{1}{2} \chi_{\perp} H - \frac{1}{2} \chi_{\perp} H \sin 2\varphi, \quad (16)$$

$$M_{\perp} = 2^{-1/2} [\sigma_{D\perp} + (\sigma_{D\perp} - \sigma_{D\parallel}) \sin 2\varphi] (\cos \varphi - \sin \varphi) + \frac{1}{2} \chi_{\perp} H \cos 2\varphi. \quad (17)$$

The thermodynamic potential (11) as a function of the angle of the rotation of the antiferromagnetic vector l away from the [100] axis takes in this case the form

$$\Phi = -\frac{1}{2} \chi_{\perp} H_{D\perp}^2 + [\chi_{\perp} H_{AE}^2 + \frac{1}{2} \chi_{\perp} (H_{D\perp} - H_{\tau})^2] \sin^2 2\varphi - 2^{-1/2} \sigma_{D\perp} H (\cos \varphi + \sin \varphi) + 2^{-1/2} [\sigma_{D\perp} - \sigma_{D\parallel}] H (\cos \varphi + \sin \varphi) \sin 2\varphi - \frac{1}{4} \chi_{\perp} H^2 (1 - \sin 2\varphi). \quad (11a)$$

We note that formulas (16) and (17) coincide with formulas (6) and (7) if we put in the latter $\chi_{\parallel} = 0$ (but if we assume at the same time that $\chi_{\parallel} H_{D\parallel} = \sigma_{D\parallel}$). However, the expressions for the anisotropy energy in the thermodynamic potentials (1a) and (11a), and also in (5) and (15), are different.

Comparing formulas (15) and (14), we see that the expression in the brackets in the first term of Eq. (15) is equal to half the square of the gap in the AFMR spectrum. In the subsequent calculations we used the gap value obtained by Richards^[5], namely $3.3 \pm 0.05 \text{ cm}^{-1}$ at $T = 4.2^\circ \text{K}$; when recalculated in terms of a g-factor equal to 2, this corresponds to a squared magnetic field 160 kOe^2 .

For different values of $Q = (\sigma_{D\perp} - \sigma_{D\parallel})/\sigma_{D\perp}$ we used a computer to determine the plots of $\varphi(H)$ from (15), and the theoretical plots of $M_{\parallel}/\sigma_{D\perp}$ and $M_{\perp}/\sigma_{D\perp}$ from (16) and (17), respectively. Figure 9 shows a comparison of the experimental plots of $M_{\parallel}/\sigma_{D\perp}$ and $M_{\perp}/\sigma_{D\perp}$ against the relative field $H/H_{D\perp}$ with the theoretical plots calculated for different values of Q .

$T_N, ^\circ\text{K}$	$\chi_{\perp} \cdot 10^6$, cgs emu/mole	$\sigma_{D\perp}$, cgs emu/mole	$\sigma_{D\parallel}$, cgs emu/mole	H_E , kOe	$H_{D\perp}$, kOe	H_{τ} , kOe	Source
73.2 ± 0.1	—	$175 \pm 10^*$	—	—	—	—	[3]
73.3 ± 0.1	6.55 ± 0.3	172 ± 5	—	1210	27.2	$9.8 \pm 1^{**}$	[5]
—	6.02 ± 0.05	161.5 ± 0.3	69 ± 4	1130	26.6	—	[6]
73.3 ± 0.1	6.2 ± 0.1	169 ± 2	57 ± 4	1170	27.2	9.3 ± 0.6	[7] Present work

*Matarrese and Stout^[3] cite in their discussion a value $\sigma_{D\perp} = 350$ cgs emu/mole, but the experiment results of their paper correspond to $\sigma_{D\perp} = 175 \pm 10$ cgs emu/mole.

**The value of H_{τ} was obtained by reducing the experimental data of Richards^[5] with the aid of expression (14) for the antiferromagnetic-resonance frequency and the value $H_{D\perp} = 27.2$ kOe.

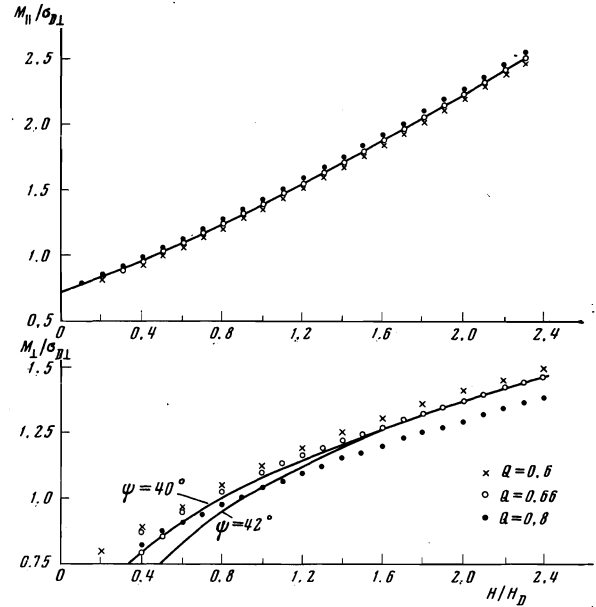


FIG. 9. Comparison of theoretical plots of $M_{\parallel}/\sigma_{D\perp}$ and $M_{\perp}/\sigma_{D\perp}$ (points) at different parameters Q with the experimental curves.

It is seen from the data obtained that the theoretical curves agree well with the experimental ones at $Q = 0.66 \pm 0.02$. In accordance with the statements made above, we have therefore assumed that in strong fields it is possible to compare the experimental $M_{\perp}(H)$ curves for $\psi = 40$ and 42° with the theoretical curve calculated for $\psi = 45^\circ$. The value obtained for Q corresponds to the following value of the longitudinal weak ferromagnetism:

$$\sigma_{D\parallel} = 57 \pm 4 \text{ cgs emu/mole}$$

The values of the effective field that cause the transverse and longitudinal weak ferromagnetism are in this case

$$H_{D\perp} = 27.2 \pm 0.2 \text{ kOe}, \quad H_{\tau} = 9.3 \pm 0.6 \text{ kOe}.$$

A plot of the dependence of the angle of rotation of the antiferromagnetic vector l away from the [100] axis, for values of $\sigma_{D\perp}$ and $\sigma_{D\parallel}$ obtained by us, is shown in Fig. 10.

In conclusion, we present a summary of the experimental values of T_N , χ_{\perp} , $\sigma_{D\perp}$, and $\sigma_{D\parallel}$ obtained by different authors (see the table).

The somewhat smaller value of $\sigma_{D\parallel}$ obtained in our experiments may be due to the fact that no account was taken of χ_{\parallel} in the comparison of the experimental and theoretical curves.

In our experiments at $H \parallel [110]$ and $H < 12$ kOe, we

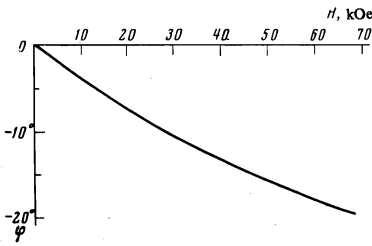


FIG. 10. Dependence of the angle of rotation of the antiferromagnetic vector L away from the $[100]$ axis on the magnetic field $H \parallel [110]$.

observe the linear relation $M_{\parallel}(H) = \sigma' + \chi' H$, where $\sigma' = (0.72 \pm 0.01)\sigma_{D\perp}$ and $\chi' = (0.64 \pm 0.02)\chi_{\perp}$. In the presented discussion of the results, based on the anisotropy of the g -factor, it was assumed that $\chi_{\parallel} = 0$; however, if we assume that $\chi_{\parallel} \neq 0$, then at $H < 12$ kOe and $H \parallel [110]$ we get $\chi' = (\chi_{\perp} + \chi_{\parallel})/2$ (see (6)). Then the value of χ_{\parallel} estimated from the experimental data is $\chi_{\parallel} = 24\% \chi_{\perp}$; the calculated value of $\sigma_{D\parallel}$ is accordingly increased ($\sigma_{D\parallel} = 70 \pm 4$ cgs emu/mole, $H_{D\parallel} = 11.4 \pm 0.6$ kOe) (see (5) and (6)), and the angle of rotation of the antiferromagnetic vector L away from the $[100]$ axis decreases with increasing H .

5. We turn now to the results obtained by us at $T > 4.2^{\circ}\text{K}$. As seen from Fig. 6, when T approaches T_N , the value of M_{\perp} measured at $\psi = 40^{\circ}$ decreases continuously and becomes less than 20% of M_{\parallel} even at $T = 65^{\circ}$. This means that at high temperatures the magnetization vector assumes a direction almost parallel to the applied magnetic field. This can easily be understood if it is recognized that at high temperatures, when L decreases, it is possible to neglect in the thermodynamic potential (1) all the terms of order higher than the first in L_{α} . Then

$$\Phi = \frac{1}{2}BM^2 - e(M_y \cos \varphi + M_x \sin \varphi) - MH. \quad (18)$$

If the magnetic field is applied at an angle ψ to the $[010]$ direction, then we obtain from the minimum of (18)

$$\sin(\varphi - \psi) = 0, \quad M_x/M_y = L_y/L_x = H_x/H_y, \quad (19)$$

i.e., $M \parallel H$, and the antiferromagnetic vector L is directed at an angle $\varphi = \psi$ to the $[100]$ axis; in this case

$$M_{\parallel} = e/B + H/B, \quad M_{\perp} = 0.$$

At high temperatures, therefore the magnetic properties of the crystal should become isotropic in the basal plane. The magnetization follows the magnetic field at all times. However, the vector L rotates away from the direction perpendicular to H at $H \parallel [010]$, toward the direction parallel to H when $H \parallel [110]$. Comparing these theoretical conclusions with our results, we see that a state that is practically fully isotropic with respect to the spontaneous moment is realized at temperatures 2–2.5° below T_N ($T_N = 73.3 \pm 0.1^{\circ}\text{K}$). By applying the field H parallel to $[010]$, we observe a "transverse" weak ferromagnetism $\sigma_{D\perp}$, and at $H \parallel [110]$ we observe a "longitudinal" weak ferromagnetism $\sigma_{D\parallel}$. As seen from Fig. 7, at $T_N - T < 2^{\circ}\text{K}$ we have for the spontaneous moment $\sigma_{D\perp} \approx \sigma_{D\parallel}$.

We note that the value of σ at $T = 72^{\circ}\text{K}$ is still of the order of 30% of its value at helium temperatures. With decreasing temperature, the picture of the rotation of the vector L gradually changes, assuming the form described in detail above (for $T = 4.2^{\circ}\text{K}$).

6. In the immediate vicinity of T_N , in accordance with the existing theory of inducing antiferromagnetic

ordering by a magnetic field^[9], χ_{\perp} passes through a sharp maximum. The obtained experimental values of χ_{\perp} in the temperature interval from 69 to 71.5°K are adequately described by the formula

$$\chi_{\perp} = 6.4 \cdot 10^{-3} \left(1 - \frac{A}{T_N - T} \right), \quad A = (0.029 \pm 0.002)^{\circ}\text{K}.$$

In the temperature interval from 74 to 72°K, the experimental values are described by the formula

$$\chi_{\perp} = 6.4 \cdot 10^{-3} \left(1 + \frac{B}{T_N - T} \right), \quad B = 0.061 \pm 0.002^{\circ}\text{K}.$$

The numerical values of the constants agree well with the data of^[10] and confirm, within the limits of the accuracy of our experiment, the conclusions of the thermodynamic theory ($B \approx 2A$).

Thus, we have demonstrated experimentally in this study that if a magnetic field parallel to the $[110]$ axis is applied to an NiF_2 crystal, then the antiferromagnetic vector L is deflected away from $[100]$ (or $[010]$) axis, and tends to become perpendicular to the applied field. In a field $H = 65$ kOe, the vector L rotates through an angle $\varphi = 20^{\circ}$. A comparison of the obtained experimental plots of the magnetizations $M_{\parallel}(H)$ parallel to the magnetic field and $M_{\perp}(H)$ perpendicular to the magnetic field against the magnetic field shows that a "longitudinal" weak ferromagnetism exists in NiF_2 .

The calculation of $M_{\parallel}(H)$ and $M_{\perp}(H)$ in the Moriya-Turov model, in which account is taken of the onset of weak ferromagnetism as a result of the g -factor anisotropy, and a comparison of the computer-calculated curves with the experimental curves made it possible to determine the values of the transverse ($\sigma_{D\perp} = 169 \pm 2$ cgs emu/mole) and longitudinal ($\sigma_{D\parallel} = 57 \pm 4$ cgs emu/mole) weak ferromagnetism.

We have shown that a parallel magnetic susceptibility ($H \parallel L$) can exist in NiF_2 , with a value $\chi_{\parallel} \approx (1.6 \pm 0.2) \times 10^{-3}$ cgs emu/mole. When χ_{\parallel} is taken into account, the longitudinal weak ferromagnetism takes on the value $\sigma_{D\parallel} = 70 \pm 4$ cgs emu/mole.

At high temperatures (close to T_N) and at any direction of the magnetic field, the magnetization vector is directed along the field and its value is independent of the angle ψ between the field and the $[100]$ axis. In this case, the longitudinal weak ferromagnetism is observed in the weak fields and is equal in magnitude to the transverse weak ferromagnetism, in agreement with Dzyaloshinskiĭ's theory.

In conclusion, the authors thank P. L. Kapitza for interest in the work and I. E. Dzyaloshinskiĭ for fruitful discussions. The authors also thank S. V. Petrov for growing and providing the NiF_2 crystals.

⁹We used a Hall pickup constructed at the Electrotechnical Institute of the Slovak Academy of Sciences. The authors are grateful to Dr. Hlasnik for supplying this pickup.

¹I. E. Dzyaloshinskiĭ, Zh. Eksp. Teor. Fiz. 33, 1454 (1957) [Sov. Phys.-JETP 6, 1120 (1958)].

²I. E. Dzyaloshinskiĭ, Dissertation, IFP AN SSSR, 1957.

³L. M. Matarrese and J. W. Stout, Phys. Rev., 94, 1792 (1954).

⁴R. A. Alikhanov, Zh. Eksp. Teor. Fiz. 37, 1145 (1959) [Sov. Phys.-JETP 10, 814 (1960)].

- ⁵ P. L. Richards, *J. Appl. Phys.*, **34**, 1237 (1963).
⁶ A. H. Cooke, K. A. Gehring, and R. Lazenby, *Proc. Phys. Soc.* **85**, 967 (1965).
⁷ R. J. Joenk and R. M. Bozorth, *Proc. of the Intern. Conf. on Magnetism*, Nottingham, 1964.
⁸ T. Morija, *Phys. Rev.*, **117**, 635 (1961).
⁹ E. A. Turov, *Fizicheskie svoystva magnitouporyado-*

chennykh kristallov (Physical Properties of Magnetically Ordered Crystals), 1963.
¹⁰ S. Foner, *Rev. Sci. Instr.*, **37**, 468 (1959).

Translated by J. G. Adashko
153